IRIS AperTO

UNIVERSITÀ DEGLI STUDI DI TORINO

AperTO - Archivio Istituzionale Open Access dell'Università di Torino

The characterization of the VNxHy defects in diamond through the infrared vibrational spectrum. A quantum mechanical investigation

This is a pre print version of the following article:

Original Citation:

Availability:

This version is available http://hdl.handle.net/2318/1685804 since 2019-01-07T11:24:58Z

Published version:

DOI:10.1016/j.carbon.2018.02.045

Terms of use:

Open Access

Anyone can freely access the full text of works made available as "Open Access". Works made available under a Creative Commons license can be used according to the terms and conditions of said license. Use of all other works requires consent of the right holder (author or publisher) if not exempted from copyright protection by the applicable law.

(Article begins on next page)

13 December 2025

The Characterization of the VN_xH_y Defects in Diamond through the Infrared Vibrational Spectrum. A Quantum Mechanical Investigation.

Simone Salustro,[1] Francesco Silvio Gentile,[1] Alessandro Erba,[1]
Philippe Carbonniére,[2] Khaled E. El-Kelany,[3] and Roberto Dovesi[1]

[1] *Dipartimento di Chimica, Università di Torino and NIS (Nanostructured Interfaces and Surfaces) Centre, Via P. Giuria 5, 10125 Torino, Italy*
[2] *Equipe de Chimie Physique, IPREM UMR5254, Université de Pau et des Pays de l'Adour, 64000 Pau, France*
[3] *CompChem Lab, Chemistry Department, Faculty of Science, Minia University, 61519 Minia, Egypt*

(Dated: May 27, 2018)

The six possible VN_xH_y defects in diamond (a vacancy surrounded by x = 1 to 3 a vacancy surrounded by x=1 to 3 nitrogens and y=1 to 4-x hydrogens) are investigated at the quantum mechanical level by using the periodic supercell approach (64 atoms), an *all electron* Gaussian-type basis set, and hybrid functionals. It turns out that steric hindrance and short range repulsion is not such to prevent hydrogen atoms (up to 3 in VNH_3) from fitting in the V cavity and saturating the dangling bonds of the carbon atoms first neighbors of the vacancy. All the investigated systems present specific IR spectra, with bending and stretching peaks above the nearly continuous band (from 400 to about 1340 cm^{-1}) resulting from the perturbation of the perfect diamond spectrum by the vacancy and the nitrogen substitutions. These peaks, ranging from 1340 to 1700 cm^{-1} (bending; data refer to the harmonic approximation) and from 3100 to nearly 4000 cm^{-1} (stretching), might be considered fingerprints of the various defects. The C–H anharmonicity, evaluated numerically, turns out to be very sensitive to the N and H load, ranging from -202 cm^{-1} (red shift of the triplet state of VNH) to +57 cm^{-1} (blue shift of the symmetric stretching in VNH_3).

1. INTRODUCTION

Hydrogen is one of the most important impurities in diamond. It is included during the growth of natural diamond as well as in chemical vapour deposition (CVD) processes. It is certainly present at the surfaces; a non minor fraction, however, is also thought to be incorporated in the bulk. Hydrogen atoms are supposed to be present in several defects[1,2], involving vacancies and/or nitrogen atoms isolated or aggregated. It is mostly identified through its infrared (IR) active modes (stretching and bending), although probably not all hydrogen atoms present in diamond are IR active.

In 2002 Briddon and coworkers[3] published a review about hydrogen in diamond, where a set of different defects containing hydrogen are simulated. Five years later (2007) an experimental review by Fritsch[4] appeared, where an overview of the peaks that "have been at least tentatively attributed to H-related defects"[4] is given. As a matter of fact, the one-to-one correspondence between the many peaks that can reasonably be attributed to the presence of hydrogen in a specific local defect is still lacking. For example, only very recently (2014) Briddon and coworkers[5] have been able to reliably attribute the experimental peaks at 1405 and 3107 cm^{-1}, that are observed in almost all types of *Ia* natural diamonds[1,4,6–8], to the VN_3H defect[9] (a carbon vacancy where 3 of the 4 first neighbors are nitrogen atoms and the fourth is saturated with hydrogen).

In particular, we have been unable to find indications concerning the IR spectra that can be generated by combining H and N in the vacancy: how many H atoms can *fit* in the vacancy when various N atoms are present? Is there enough *room* for the progressive saturation of the fraction of first neighbors of the vacancy occupied by carbons? Is the progressive saturation with hydrogen atoms exothermic for any concentration of nitrogens, or is the steric and/or electronic hindrance (the latter due to the presence of the lone-pairs on the N atoms) preventing the high loading? How different is the IR spectrum of the various VN_xH_y compounds and spin states? More important, is the intensity of the C-H bending and stretching modes large enough to allow to recognize these modes as a fingerprint of a specific defect, as it is the case of VN_3H (see Ref. 4)?

In 2015 Peaker and coworkers[10] investigated electronic and vibrational features of two of the systems discussed in this work: VN_2H_2 and VN_2H (the latter also in its negative charged form). Their vibrational frequencies are obtained through a finite difference approximation for the evaluation of second derivatives of energy with respect to atomic coordinates. As reported in their work, "the eigenvalues of the dynamical matrix provide the frequencies which are quasi-harmonic due to the inclusion of small components of anharmonic incurred from the finite displacement of the atoms".[10] According to their PBE calculations, the C–H stretching modes are expected to be at 3540 (symmetric) and 3370 (anti-symmetric) cm^{-1} for the former, and at 3050 cm^{-1} for the latter.

From the experimental side, it is clearly very difficult to know how many different defects containing hydrogen are present in the sample, and at which concentration, and how they are combined with other defects.

From the simulation point of view it is possible to define *a priori* the kind of defects present in the bulk. Other limitations prevent however the simple identification of

the experimental peaks with the simulated ones. The three most important are related to i) the use of functionals (LDA, GGA) that are known to poorly perform with open-shell systems, and in describing hydrogen atoms for which the self-interaction error is particularly severe[11]; ii) inaccuracies in the models for treating the vibrational modes (harmonic approximation), that in this particular case clearly fail due to the strong anharmonicity of the C–H stretching; iii) unavailability of the IR intensities. Some of these limitations deeply affect the previous quantum-mechanical simulations of hydrogen-containing defects.

In a series of previous works[9,12–20] some of the present authors have proposed the quantum-mechanical characterization of several point-defects in diamond. Here we extend our preliminary investigation on the structural, electronic and spectroscopy features of the VN_3H defect[9] by considering the entire set of VN_xH_y (x= 1 to 3, y=1 to 3) situations. The present study represents, to our knowledge, the most extensive investigation of this family of compounds and of their spectroscopic features. Moreover, it also introduces important improvements with respect to previous treatments (the three limitations mentioned above are totally or in part eliminated). Six different systems (namely VNH_1, VNH_2, VNH_3; VN_2H_1, VN_2H_2; VN_3H), whose general structure is reported in Figure 1, have been studied by using a hybrid functional (B3LYP), a Gaussian-type basis set and the supercell scheme (here the analysis is limited to cells containing 64 atoms, as the hydrogen related modes, on which we focus here, are very localized and the effect of the lateral interaction between defects belonging to different cells on these modes is extremely small).[9,19] All the investigated systems present specific IR spectra, with peaks that can be used for the characterization of each one of these defects. In particular, the C-H bending and stretching modes can be considered as spectroscopic fingerprints of the system. These modes span about 300 (bending) and 1000 cm^{-1} as a function of the number of hydrogen and nitrogen atoms around the vacancy. Also anharmonicity (here investigated for the stretching modes) is quite sensitive to the nitrogen and hydrogen load and to the spin state of the system.

The paper is structured as follows. In Section 2 information on the adopted computational setup is provided. Subsection 2.1 is devoted to the vibrational frequencies computed in the harmonic approximation, and to the analytical estimation of the IR intensities. Subsection 2.2 illustrates how the anharmonic contribution to the C-H stretching mode is computed by solving numerically the corresponding one dimensional Schrödinger equation. Section 3 is organized in two parts. Subsection 3.1 is devoted to the equilibrium geometry of the studied defects, to their charge distribution and to their band structure. In Subsection 3.2, the vibrational features of the defects are reported and analyzed, both at the harmonic and anharmonic (for the stretching) level. Finally, in Section 4 some conclusions are drawn.

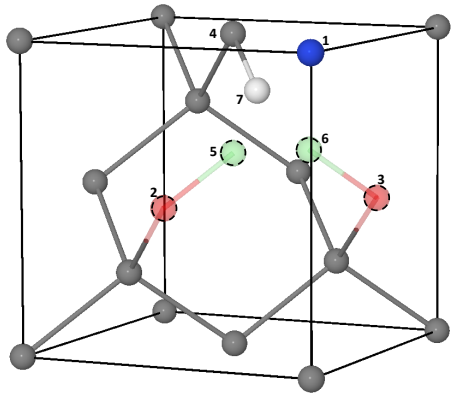

FIG. 1: Schematic representation of the VN_xH_y conventional cells. Red position can either be occupied by N (up to x, spanning from 1 to 3) or C. The green positions are occupied by H atoms down to 8-y. According to this scheme, for the six systems here considered, we have: N in 1, C in 2 and 3, H in 7 for VNH; N in 1 and 2, C in 3, H in 7 for VN_2H; N in 1, 2 and 3, H in 7 for VN_3H; N in 1, C in 2 and 3, H in 7 and 6 for VNH_2; N in 1, C in 2 and 3, H in 7, 6 and 5 for VNH_3; N in 1 and 2, C in 3, H in 7 and 6 for VN_2H_2.

2. COMPUTATIONAL MODELS AND DETAILS

Calculations have been performed by use of the B3LYP global hybrid functional,[21,22] as implemented in the CRYSTAL program.[23] In a recent work some of the present authors have shown that weak dispersive interactions only marginally affect the description of covalent system as diamond.[20]

Turning now to the description of the electron density, an *all electron* basis set of Gaussian-type functions has been adopted (Pople's 6-21G) for carbon and nitrogen atomic species; the exponent of the most diffuse *sp* shell is 0.23 (C) and 0.30 (N) $Bohr^{-2}$. The 6-31G basis set[24] has been used for hydrogen. In order to simulate the presence of a vacancy in the defective structure, a complete removal of the atom of interest (nucleus, electrons, basis set) has been performed. We have shown in previous studies that a "ghost" atom approach whould lead to similar results concerning structural, electronic and spectroscopic features.[12,13,20]

The truncation of the Coulomb and exchange infinite lattice series is controlled by five thresholds T_i (see Ref. 25 for more details), which have been set to 8 (T_1-T_4) and 16 (T_5). The convergence threshold on energy for the self-consistent-field (SCF) procedure has been set to 10^{-8} Hartree for structural optimizations and to 10^{-10} Hartree for vibration frequency calculations.

The DFT exchange-correlation contribution to the Fock matrix has been evaluated by numerical integration over the unit cell volume. Radial and angular points for the integration grid are generated through Gauss-Legendre radial quadrature and Lebedev two-dimensional angular point distributions. The default pruned grid with 75 ra-

dial and 974 angular points has been used, whose accuracy can be measured by comparing the integrated charge density of each system with the total number of electrons in the unit cell: as an example, the charge density of VNH_1 is 380.004, while the total amount of electrons is 380.
Reciprocal space has been sampled using a Γ-centered regular Pack-Monkhorst[26] sub-lattice (controlled by the `SHRINK` keyword, see the CRYSTAL User's Manual[25]) with a "shrinking factor" (IS[25]) equal to 8, that corresponds to 8×8×8=512 **k**-points in the First Brillouin Zone (FBZ) (260 by exploiting the *time reversal symmetry*). The six defective systems here considered belong to one of the following symmetry point-groups: C_1, C_s, C_{2v} and C_{3v}. Exploitation of symmetry reduces the **k**-points to be sampled in the FBZ from 260 (C_1) to 150 (C_s), 105 (C_{2v}) and 65 (C_{3v}).

2.1. Harmonic frequencies and the IR spectra

Frequencies at the Γ point are obtained within the harmonic approximation by diagonalising the mass-weighted Hessian matrix, W, whose elements are defined as[27–31]

$$W^{\Gamma}_{\alpha i,\beta j} = \frac{H^{\mathbf{0}}_{\alpha i,\beta j}}{\sqrt{M_\alpha M_\beta}} \quad \text{with} \quad H^{\mathbf{0}}_{\alpha i,\beta j} = \left(\frac{\partial^2 E}{\partial u^{\mathbf{0}}_{\alpha i} \partial u^{\mathbf{0}}_{\beta j}} \right) , \tag{1}$$

where M_α and M_β are the masses of atoms associated with the i and j atomic coordinates. Once the Hessian matrix, $\mathcal{H}_{\alpha i,\beta j}$, has been calculated, frequency shifts due to isotopic substitutions can be calculated readily, at no computational cost, by changing masses in Eq. 1.
Energy first derivatives with respect to the atomic positions, $v_{\alpha,j} = \partial E / \partial u_{\alpha,j}$, are calculated analytically for all the $u_{\alpha,j}$ coordinates (E is the total energy, $u_{\alpha,j}$ is the displacement coordinate with respect to the equilibrium, α labels each atom), whereas second derivatives at $\vec{u} = 0$ are calculated numerically using a single displacement along each coordinate (N=2, the central point and one point on the right side of the parabola):

$$\left[\frac{\partial v_{\alpha j}}{\partial u_{\beta i}} \right] \approx \frac{v_{\alpha j}(0, \dots, u_{\beta i}, \dots)}{u_{\beta i}} \tag{2}$$

or averaging two displacements (N=3):

$$\left[\frac{\partial v_{\alpha j}}{\partial u_{\beta i}} \right] \approx \frac{v_{\alpha j}(0, \dots, u_{\beta i}, \dots) - v_{\alpha j}(0, \dots, -u_{\beta i}, \dots)}{2 u_{\beta i}} \tag{3}$$

Previous calculations[27,32,33]have shown that in bulk systems the influence of both u and N is very small (less than 1 cm^{-1}) when H atoms are not present; much larger effects have been found for the O-H stretching in katoite[34], brucite[35,36] and diaspore[37]. More generally, anharmonicity is large in all cases in which hydrogen atoms are involved (*vide infra*)[38,39]. Integrated intensities for IR absorption $\mathcal{I}_p$ are computed for each mode p by means of the mass-weighted effective-mode Born-charge vector $\vec{Z}_p$[40,41] evaluated through a Coupled-Perturbed-Hartree-Fock/Kohn-Sham (CPHF/KS) approach:[42,43]

$$\mathcal{I}_p \propto \left| \vec{Z}_p \right|^2 . \tag{4}$$

2.2. The anharmonicity of the C-H stretching mode

When both the fundamental frequency ω_{01} and the first overtone ω_{02} of a mode are available, the anharmonicity constant $\omega_e \chi_e$ can be obtained through the formula (see Ref. 36 for more details):

$$\omega_e \chi_e = \frac{(2\omega_{01} - \omega_{02})}{2} \tag{5}$$

that allows also the definition of the harmonic frequency ω_e as:

$$\omega_e = \omega_{01} + 2\omega_e \chi_e \tag{6}$$

The importance of anharmonicity in H containing systems appears evident by looking at the anharmonicity constant $\omega_e \chi_e$ of some simple diatomic molecules such as H_2, HF, HCl and HBr, where $\omega_e \chi_e$ is 121, 90, 53 and 45 cm^{-1}, respectively.[44] As regards the C-H stretching, anharmonicity is estimated to be around 100-200 cm^{-1} for many organic molecules.[45,46]
The very large anharmonicity of the C-H, N-H and O-H stretching modes can be estimated by taking advantage of their independence from the other normal modes.[33–35,39]
A scheme has been implemented in the CRYSTAL code that solves numerically the one-dimensional Schrödinger equation when the potential energy, evaluated for a set of 7 points along the C-H coordinate, is fitted with a sixth order polynomial.[47] The explored interval for the present case goes from -0.8 to +1.0 Å with respect to the equilibrium position. The explored energy range is about 1.1 eV. The results vary by less than 1 cm^{-1} when a much richer set of points (26) is used in the same interval.
Unfortunately this simple and effective scheme cannot be extended to the other hydrogen modes, such as bending, because in this case the separability with respect to the other modes is lost. In this case a full anharmonic treatment is required.

3. RESULTS

Let us summarize the electronic situation of the systems we are considering in the present study. In the vacancy V there are 4 unpaired electrons, that can generate three different states characterized by S_z=0, 1 and 2 (four spin up, three up and one down, two up and two down); we can call these states quintuplet, triplet and singlet.

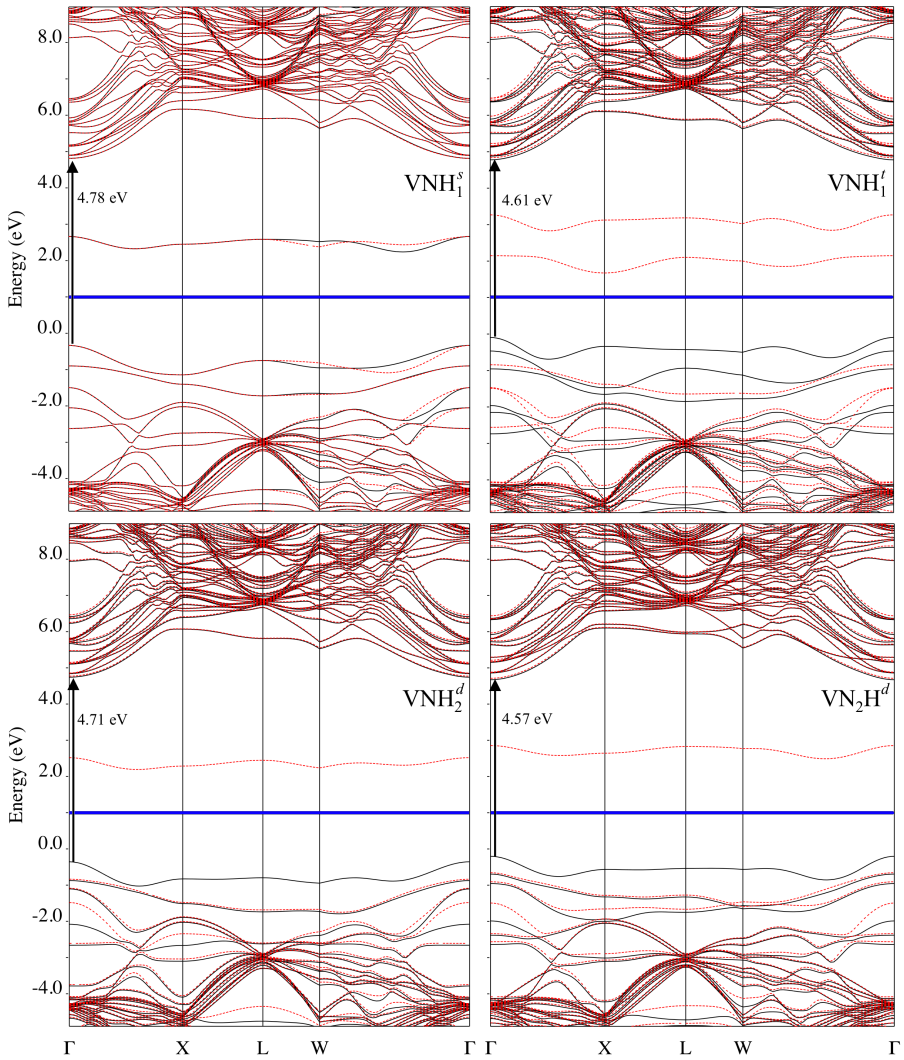

FIG. 2: B3LYP band structures of the open-shell VN_xH_y defects for the S_{64} supercells. The spin configuration is denoted by the supercript: singlet (s), doublet (d) and triplet (t). Continuous black lines represent α energy levels, whereas dotted red lines refer to β energy levels. The horizontal blue line marks the position of the Fermi energy level. The optical transition has been represented by the black arrow.

It should be underlined that the unpaired electrons remain localized to a large amount on the carbon atoms, as it should be, if and only if a sufficiently large amount of "exact" Hartree Fock (HF) exchange is included in the Hamiltonian or functional. In HF the localization is complete (one electron on each carbon atom); in "hybrid" functionals, such as B3LYP or PBE0 (very rarely adopted in previous studies for these systems), the localization remains large (about 0.8 $|e|$ on each unsaturated carbon atom, according to a Mulliken partition of the charge density). LDA and various versions of GGA, like PBE, are unable to localize these electrons, and the solution turns out, for many of the defects in diamond, to be metallic, in contrast with experimental evidence. The energy difference between the singlet and the triplet, evaluated at the B3LYP 6-21G level, is quite small (0.13 eV), whereas the quintuplet is less stable by about 1.4 eV.[12,13] At the other extreme with respect to the vacancy, in VN_4 (the B defect), "border" atoms are nitrogens, with a lone pair each protruding towards the vacancy, so that the ground state has a closed shell configuration.

For the systems here investigated, the carbon atoms that are first neighbors of the vacancy are progressively substituted by nitrogen, and the remaining carbon dangling bonds are partially or totally saturated by hydrogen atoms. When only one nitrogen is inserted, then three VNH_y systems can be generated, with y=1, 2 or 3. In VNH_1, two unpaired electrons remain, that can combine to give a triplet (S_z=1) or a singlet (S_z=0) state. In VNH_2 the only spin state available is a doublet, whereas VNH_3 has a closed-shell ground state. When two nitrogen atoms are first neighbors of the vacancy, two cases

are possible: VN_2H_1, with a doublet open-shell configuration, and VN_2H_2, a closed-shell. Also the last case here considered, VN_3H, has a closed-shell ground state. The relative stability of the different spin states, and the stability of the various defects when the number of nitrogen and hydrogen atoms in the vacancy is increasing, are among the issues that will be discussed in this section.

3.1. Geometry, charge and spin densities, and band structure

As we are mainly interested in the behavior of the C-H groups, we reported in Table I only two geometrical data, namely the C-H and the H-H distances (when applies). The former is equal to 1.07 Å when a single hydrogen atom is present, to 1.05 Å when there are two H atoms in the cavity, and to 1.03 Å in the case with three H atoms; the shortening is a consequence of the repulsion between hydrogen atoms. The H-H distance in the cavity is always around 1.26 Å, sufficiently short to generate some repulsion. The polarity of the C-H bond is large when a single hydrogen is present (+0.23 $|e|$ on H and -0.16 $|e|$ on the C_1 atom, linked to H, in the two VNH states), and reduces progressively when the number of H atoms increases (+0.21 and +0.17 $|e|$, -0.15 and -0.12 $|e|$ in VNH_2 and VNH_3, respectively) so as to reduce the mutual electrostatic repulsion among them. The polarity increases, for fixed number of H atoms, when the number of N atoms increases, (+0.23, +0.27, +0.31 $|e|$ for H, and -0.16, -0.17 and -0.18 $|e|$ for C_1 in going from VNH^s to VN_2H^d and to VN_3H). The net atomic charge of nitrogen varies from -0.42 to -0.47 $|e|$, and is nearly completely compensated by its three carbon first neighbors. When the system is spin polarized, the spin density is essentially localized on the unsaturated carbon atoms: the table shows that the amount of spin density on H, N and C_1 is very small, the maximum being +0.08 $|e|$ for a system with two uncoupled electrons (the VNH^t case). Also the C-H bond population is nearly constant along the series; it is interesting to note the small but positive N-H bond population (attractive) and the small and negative H-H bond population (repulsive).

Three of the investigated systems present a closed-shell electronic structure; their band structures are very similar, with band gaps that reduce from 5.50 eV (VNH_3), to 5.30 eV (VN_2H_2) to 5.22 eV (VN_3H) when the number of nitrogen atoms increases from 1 to 3. The limiting case VN_4 (the so called B-center), has a band gap even smaller (5.06 eV). In all cases, the energy levels of the hydrogens are down in the occupied manifold, whereas the valence bands are always due to the lone pairs of the nitrogen atoms. The band structure of the closed-shell systems are not further discussed.

The other three systems do have a spin polarized ground state: VNH has 2 unpaired electrons, that can couple to give a triplet (t) or a singlet (s); the latter is slightly more stable than the former by 0.14 eV, as shown in Table II. Their band structure is given in the two top panels of Figure 2: the energy levels associated to α and β electrons are represented by continuous black and dotted red lines, respectively. Since there are two unpaired electrons, the energy levels immediately below the Fermi energy (marked by the horizontal blue line) are α and β for the singlet, and both α for the triplet. The energy dispersion of the levels occupied by the unpaired electrons is roughly 0.7 eV for both the spin states and is a measure of the interaction between defects belonging to different cells; in larger supercells, *i.e.* when the defect concentration reduces, the energy dispersion lowers. In the Figure the energy transition (starting at Γ-point) involving the highest occupied level of the defect and the first unoccupied level of the diamond host are indicated for all the reported band structures.

In the other two open shell-systems, VNH_2 and VN_2H, there is just a single unpaired electron, so that their ground state is a doublet (d). In these cases, then, there will be only one α-electron level immediately below the Fermi energy level, and one β-electron level above the Fermi energy level. The energy dispersion of the unpaired electron also in these cases is about 0.7 eV.

It is interesting to evaluate the energy required for the homolytic dissociation of the VN_xH_y system to give VN_x (the vacancy surrounded by x N atoms) and $\frac{y}{2}H_2$ molecules, according to equation

$$VN_xH_y \xrightarrow{E_H} VN_x + \frac{y}{2}H_2 \qquad (7)$$

The E_H energies are reported in Table II for all the considered systems. Looking at the series with a single nitrogen atom, *i.e.* VNH_y, it turns out that the energy required for breaking the C-H bond in VNH_1 is 1.30 eV. For the removal of the two hydrogens in VNH_2 the energy required is 2.09 eV (that gives an average of 1.05 *per* atom), whereas the extraction of the 3 hydrogens in VNH_3 requires 2.54 eV, that is only 0.85 eV *per* atom. A step-by-step homolytic dissociation procedure according to the following reaction path:

$$VNH_3 \xrightarrow{E^1_H} VNH_2 + H \xrightarrow{E^2_H} VNH + H \xrightarrow{E^3_H} VN + H$$

gives E^1_H=0.45 eV, E^2_H=0.79 eV and E^3_H=1.30 eV, confirming that the mutual steric hindrance drastically reduces the strength of the C-H bonds. In spite of that, these data show that it is energetically possible that three H atoms *fit* in the vacancy cavity. Looking now to the series with a single hydrogen atom and an increasing number of nitrogens atoms (*i.e.*, VNH, VN_2H, VN_3H), E_H increases from 1.30 to 1.42 and then to 1.66 eV; the C-H bond becomes then stronger when the number of nitrogen atoms around the vacancy increases, as a consequence of the polarization induced by the x lone pairs on the C-H bond. The effect of the lone pairs is evident also from the comparison of E_H for VNH_2 and VN_2H_2, that increases from 2.09 to 2.38 eV.

TABLE I: B3LYP structural and Mulliken population data for the various $VN_xH_y^z$ defects, where the z superscript indicates the open-shell spin state (*s*inglet, *d*oublet and *t*riplet). R_{CH} and R_{HH} are the shortest distances (in Å) between the indicated atoms, while B_{CH}, B_{NH} and B_{HH} are the corresponding bond populations (in $|e|$ units). Atomic quantities Q_X and μ_X are the net electronic and magnetic charges of atom X, respectively. C_1 is (one of) the atom saturated by H. The N-H shortest distance is always around 1.94-1.95 Å, the only exception being VNH_3 for which the distance shortens to 1.91 Å.

System	R_{CH}	R_{HH}	Q_H	Q_{C_1}	Q_N	μ_H	μ_{C_1}	μ_N	B_{CH}	B_{NH}	B_{HH}
VNH^s	1.072	-	+0.23	-0.16	-0.43	0.00	0.00	0.00	+0.29	+0.03	-
VNH^t	1.082	-	+0.23	-0.16	-0.42	-0.01	+0.08	+0.04	+0.29	+0.03	-
VNH_2^d	1.052	1.262	+0.21	-0.15	-0.45	-0.00	+0.03	+0.01	+0.32	+0.02	-0.04
VNH_3	1.034	1.265	+0.17	-0.12	-0.47	-	-	-	+0.33	+0.01	-0.06
VN_2H^d	1.075	-	+0.27	-0.17	-0.42	-0.01	+0.03	+0.02	0.30	+0.03	-
VN_2H_2	1.050	1.249	+0.25	-0.16	-0.45	-	-	-	+0.33	+0.01	-0.04
VN_3H	1.074	-	+0.31	-0.18	-0.42	-	-	-	+0.31	+0.02	-

3.2. Spectroscopic characterization

The Raman spectrum of pristine diamond is very simple: it consists of a single, sharp peak at 1332 cm^{-1}. The collective modes of the perfect diamond structure, corresponding to $\vec{k}$ points of the Brillouin Zone different from Γ in the primitive cell, have lower wavenumbers. The calculated perfect diamond single Raman peak is at 1317 cm^{-1} (B3LYP/6-21G level), 15 cm^{-1} below the experimental one. The IR spectrum of pristine diamond is even simpler because, due to symmetry constraints, no peaks are observed.

TABLE II: B3LYP/6-21 total energies, in Hartree, of the VN_xH_y and of the corresponding VN_x systems. E_H, in eV, is the homolytic dehydrogenation and formation energies evaluated according to Equations 7. Data refer to the S_{64} supercell. B3LYP/6-21G total energies of the H_2 and N_2 molecules (obtained with the CRYSTAL code) are -1.1687 Hartree and -109.3127 Hartree, respectively. If reference is done to the isolated H atom, rather than to the H_2 molecule, E_H should be increased by 2.38 eV per H atom.

System	$E_{VN_xH_y}$	E_{VN_x}	E_H
VNH^s	-2414.5406	-2413.9086	1.30
VNH^t	-2414.5357	-2413.9086	1.16
VNH_2^d	-2415.1540	-2413.9086	2.09
VNH_3	-2415.7549	-2413.9086	2.54
VN_2H^d	-2431.1837	-2430.5471	1.42
VN_2H_2	-2431.8031	-2430.5471	2.38
VN_3H	-2447.8266	-2447.181094	1.66

The IR spectrum of the pure vacancy V (see the bottom right panel of Figure 3) presents spectroscopic features below the pristine diamond Raman peak at 1317 cm^{-1}, whereas no peaks appear above. The same holds for the Raman spectrum, reported in Ref. 12.

The nitrogen substitution perturbs this situation only marginally. The highest calculated peaks for VN_1, VN_2, VN_3 and VN_4 are at 1337, 1335, 1338 and 1339 cm^{-1}, respectively, only slightly above, then, the isolated Raman peak of perfect diamond at 1317 cm^{-1}. For the systems here considered, all peaks observed above 1340 cm^{-1} must then be attributed to the presence of hydrogen.

The IR spectra of the seven systems here investigated, calculated at the harmonic level of approximation, are shown in Figure 3. The VN_3H case has already been described elsewhere.[9] All spectra show many peaks below 1340 cm^{-1}, mainly as a consequence of the reduction of the perfect diamond cubic symmetry by the vacancy, and N substitutions. The hydrogen related modes (three for each H atom) split (totally or partially) from the pure diamond+V+N manifold, and are then easily identified. The harmonic stretching and bending wavenumbers and intensities are summarized in Table III.

We begin our analysis from the bending modes. We recall that, since hydrogen is very light, the corresponding bending and stretching modes are expected to be clearly identifiable, although the first is almost always coupled to all the other modes. So we look for two "bending" modes per hydrogen atom in the graphical animation of the modes (see `www.crystal.unito.it`). In the cases in which there are two or three H atoms, some of the bending modes are at low wavenumbers, well below the Raman diamond peak: they appear at 476 cm^{-1} for VNH_2, at 471 for VN_2H_2 and at 451 cm^{-1} (twofold degenerate) and at 446 cm^{-1} for VNH_3. The table shows that all these low wavenumber modes have extremely weak (or

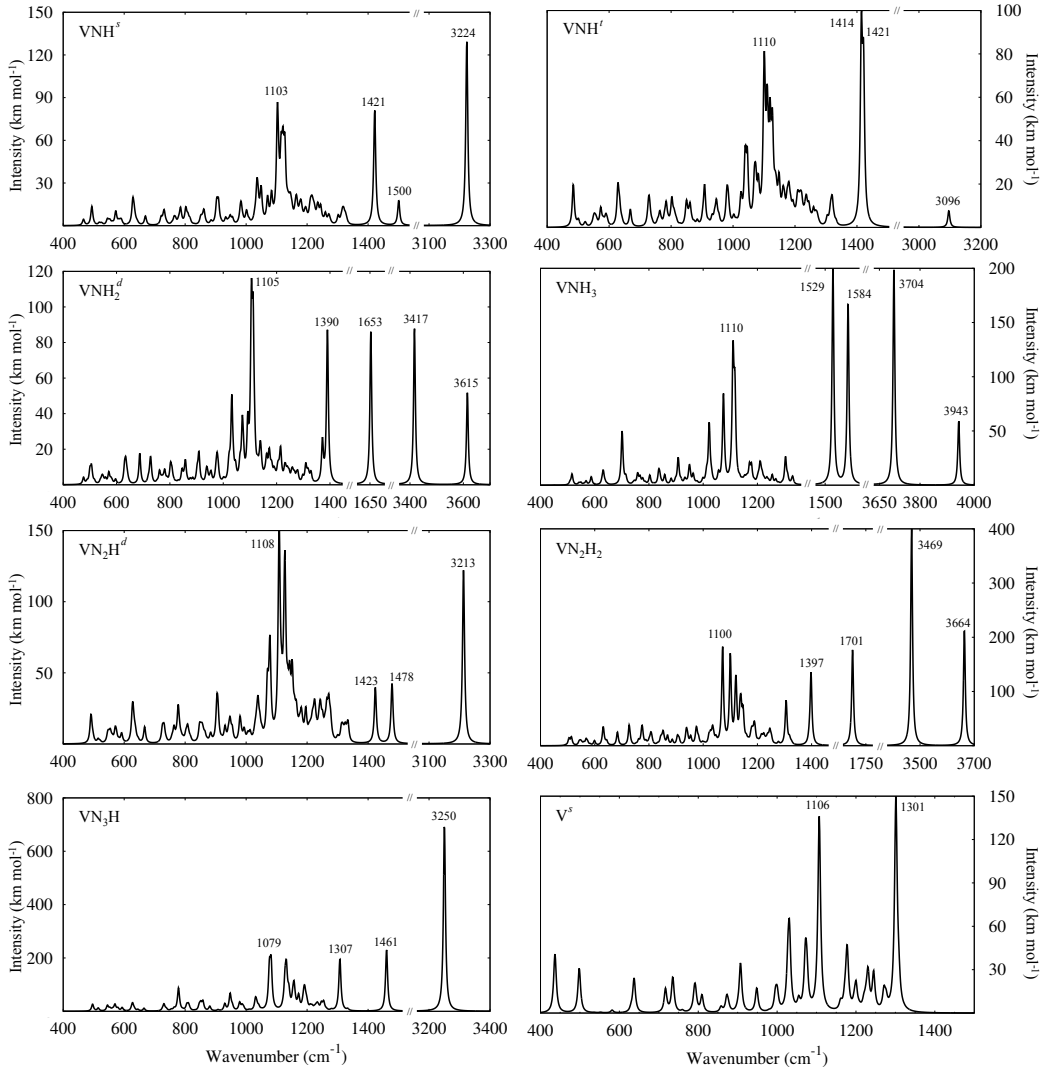

FIG. 3: B3LYP simulated infrared spectra of seven VN_xH_y defects with x equal 1, or 2 or 3. In the VNH case, two uncoupled electrons remain on two of the carbon atoms around the vacancy, that can arrange in a high spin (triplet, indicated as t), or low spin (singlet, s) configurations. In both VN_2H and VNH_2 cases there is a single uncoupled electron, and then the state is a doublet (d). The bottom right spectrum is the one of the vacancy V in its singlet s state. Wavenumbers are computed at the harmonic level. Calculations refer to the S_{64} supercell.

null) IR intensity, and cannot then be observed experimentally.

All the remaining bending modes (three for VNH_2, VN_2H_2 and VNH_3, two in all other cases, 17 in total) are in the interval 1333 – 1701 cm^{-1} and are shown in Figure 4. Two of them have negligible intensity, and three other have intensity smaller than 30% of the most intense peak (at 205 km·mol^{-1}), so that they are probably hardly detectable in the experimental spectrum. The remaining ones (11 in total) have relatively high intensity, and 5 of them span from 50 to 90% of the most intense peak. The latter belongs to VN_3H, and is very well characterized experimentally, as described in the Introduction.[4,5,9] The calculated wavenumber is at 1461 cm^{-1}, 55 cm^{-1} above the experimental value.[9] A very preliminary investigation of the anharmonic contribution, evaluated through VCI or VSCF (see Ref. 9 for definitions), in which however only the three hydrogen modes are coupled, reduces the computed wavenumber to 1446-1442 cm^{-1}. For all the other systems, we are unable to estimate the anharmonic shift of the bendings. It is fair enough to suppose that anharmonicity of the bending modes is between 0 and 55 cm^{-1} (the VN_3H value).

Combining the low intensity, and a hypothetical red shift or 20-50 cm^{-1}, that would merge some of the peaks with the "bulk" V+N nearly continuous band, one might expect to find in the experimental spectrum the 1701 (153 km·mol^{-1}) peak of VN_2H_2, the 1584 (159 km·mol^{-1}) and

TABLE III: B3LYP harmonic wavenumbers (ω, in cm^{-1}) of the C–H stretching (S_i) and bending (B_i) modes, and their relative intensities (I_{S_i} and I_{B_i}, in km·mol^{-1}). Numbers in parentheses in the VNH_3 case indicate the degeneracy of the mode. When y hydrogen atoms are present, y stretching and $2\times y$ bending modes are reported.

	Stretching				Bending							
	ω_{S_1}	I_{S_1}	ω_{S_2}	I_{S_2}	ω_{B_1}	I_{B_1}	ω_{B_2}	I_{B_2}	ω_{B_3}	I_{B_3}	ω_{B_4}	I_{B_4}
VNH^s	3224	129	-	-	1501	17	1422	81	-	-	-	-
VNH^t	3096	7	-	-	1421	58	1414	74	-	-	-	-
VN_2H^d	3213	122	-	-	1479	42	1424	39	-	-	-	-
VN_3H	3250	621	-	-	1461	205	1333	5	-	-	-	-
VNH_2^d	3615	52	3417	88	1653	50	1391	87	1372	23	476	4
VN_2H_2	3664	185	3469	346	1701	153	1398	114	1392	8	471	0
VNH_3	3943	56	3704 (2)	189	1584 (2)	159	1529	189	451 (2)	0	446	0

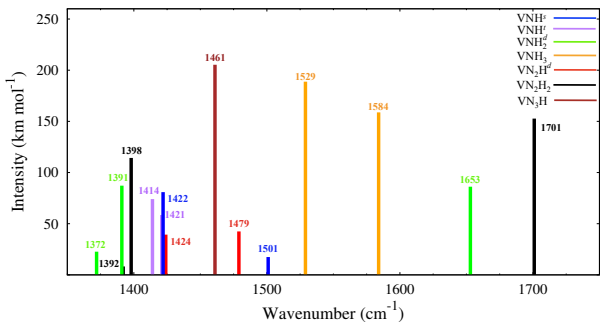

FIG. 4: Harmonic wavenumbers and intensities of the C–H bending modes of the VN_xH_y defects. Calculations refer to B3LYP/6-21G, and to the S_{64} supercell.

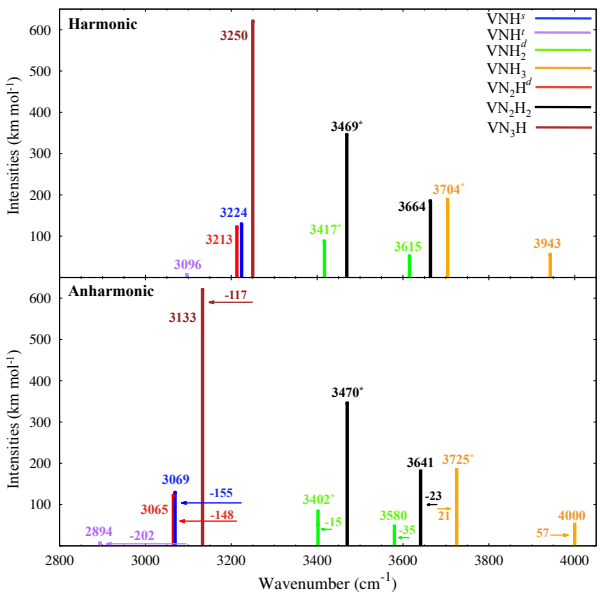

FIG. 5: B3LYP harmonic (top) and anharmonic (bottom) wavenumbers for the C-H stretching mode(s) for the VN_xH_y defects. When more than one hydrogen atom is present there are two stretching modes (symmetric, at high wavenumber, and antisymmetric, at low wavenumber, and marked with an asterisk; in VNH_3 two low wavenumber peaks are degenerate). The height of each bar is the simulated IR intensity (evaluated at the harmonic level).

the 1529 cm^{-1} (189 km·mol^{-1}) peaks, both of VNH_3. Is there something in the experimental spectra that might be attributed to these two defects?

Before answering this question, let us consider the stretching modes, that are reported in the top panel of Figure 5. The ten peaks span 850 cm^{-1}, and the intensities vary from 5 to 621 km·mol^{-1}, so that in principle it should be possible to distinguish each local situation from the others. The absolute identification with respect to experimental data remains however difficult, both because of the large variety of experimental situations spanned in the literature, corresponding probably also to many more combinations of defects than examined here, and because the simulated data are affected by a large error related to the harmonic approximation. We are in a position to correct partially for this last point, as we solved numerically the one-dimensional Schrödinger equation for the C–H coordinate, an approximation that is a minor one for this particular mode (see Subsection 2.2). The results are shown in the lower panel of Figure 5, with a horizontal arrow indicating the amount of anharmonic shift. The latter is far from being constant, and varies from -202 (redshift) to +57 (blueshift) cm^{-1}. The reason for this large difference is related to the competition between the various factors influencing the C–H stretching that i) is by itself strongly anharmonic, with a consequent red-shift; ii) the latter is enhanced by the presence of the N lone pairs on the opposite side of the vacancy that at-

tract electrostatically the H atom, that is bearing some partial positive charge; iii) the steric hindrance and short range (Pauli) repulsion, due to the presence of other H atoms in the cavity, progressively compensate for i) and ii); for the VNH_3 case, the repulsive wall due to the other H atoms is dominating and a blue shift is observed.

This large variation of anharmonicity from case to case represents a severe warning for the attempt to interpret the *reasonable* agreement obtained with pure DFT functionals at the harmonic level, as the errors due to the functional and to disregarding anharmonicity seem in some cases to cancel each other. In a family of compounds as the one discussed here, we can suppose that the first error (the use of LDA or PBE, with a consequent large self-interaction error, particularly severe for hydrogen) remains roughly constant, whereas Figure 5 shows that the second one can differ from case to case by as much as 260 cm^{-1}.

3.3. Are the VN_xH_y defects visible in the IR spectrum?

In Section 3.1 it has been shown that more than one hydrogen atom can fit in the VN_x cavity, and that the process is exothermic, in particular if compared not with the very stable H_2 molecule, but with isolated hydrogen atoms that might be present in diamond in interstitial positions (see also Table II and its caption). However, the following questions can be raised: are all these defects visible in the IR spectrum? Are the stretching and bending peaks IR active, and their intensity large enough to be visible in the experimental spectra, that are extremely complex and rich of peaks, as shown for example in the figures appearing in Ref. 4?

It is difficult to answer these questions, as many additional variables play an important role, including: i) the nature of the diamond sample, ii) the concentration of N and H in the sample, iii) the mechanisms for their migration to form the desired defect. As we do not have enough information for trying to define these additional conditions, we will adopt the (certainly not very realistic) simplifying hypothesis that *all* the defects we are discussing here do have the same concentration. The next step of the analysis is made easier by the fact that one of the systems here investigated, VN_3H, generates a couple of modes (a bending mode at 1405 and a stretching mode at 3107 cm^{-1}) that are very intense and observed in most of the experiments (see Introduction and references therein). The calculated anharmonic stretching mode of VN_3H (at 3133 cm^{-1} in Figure 5, bottom) is by far the most intense one of the full set of 10 modes reported in the figure (621 km·mol^{-1}). The second largest intensity (346 km·mol^{-1}, the antisymmetric stretching of VN_2H_2) is about 50% of the VN_3H one, followed by the symmetric mode of the same system (185 km·mol^{-1}) and the antisymmetric one of VNH_3 (189 km·mol^{-1}, one third of VN_3H). All the remaining modes have low intensity, of the order of 20% of VN_3H, or even smaller, so that probably they are hardly detectable in the stretching region of the spectra. VN_2H_2 and VNH_3 are also the most visible in the bending region, as they have intensities not much smaller that the one of VN_3H, and wavenumbers sufficiently far from the diamond+V+N continuous band (at 1529, 1584 and 1701 cm^{-1}). Hunting for similarities with the present bending wavenumbers and intensities in the many spectra reported in figure 2-6 of Ref. 4, taking also into account an hypothetical red shift of our wavenumbers, it is certainly possible to attempt some assignments. The situation appears however so undefined, that we refrain from this game, waiting for clearer experimental determinations.

As concerns previous theoretical predictions by Peaker and coworkers[10] for the C–H stretching modes, their PBE value of 3050 cm^{-1} for the VN_2H defect is not far from our B3LYP anharmonic value of 3065 cm^{-1} (see Figure 5). Larger differences are observed, instead, when the VN_2H_2 defect is considered: 3370 and 3540 cm^{-1} for anti-symmetric and symmetric C–H stretching modes, to be compared with the anharmonic values here reported of 3470 and 3641 cm^{-1}.

In summary, four of the seven systems here investigated (VNH, both *s* and *t*, VN_2H, VNH_2), can be considered hardly IR visible, or "invisible"; VNH_3 and VN_2H_2 are probably visible in the bending region but "hardly" visible in the stretching region, with the possible exception of the antisymmetric stretching of the latter.

4. CONCLUSIONS

In this work a series of hydrogen-nitrogen defects in diamond, for brevity named VN_xH_y, have been studied from a computational point of view. They consist of a carbon vacancy surrounded by at least one nitrogen atom, with at least one of the remaining dangling bonds saturated with hydrogen. This leads to 6 different models (VNH, VN_2H, VN_3H, VNH_2, VNH_3, and VN_2H_2) and 7 spin states (a triplet and a singlet state are possible for VNH, with two uncoupled electrons). Two main issues have been considered in the present study:

- are all the models here proposed realistic from the energetic point of view? So can they be inserted in the long list of defects in diamond?
- if they exist, are they also visible from the experimental point of view, in particular do they produce visible, intense IR peaks?

The answer to the first question is positive. If reference is done to the series of VN_x defects (x=1 to 3), then the saturation with hydrogen of one of the carbon atoms surrounding the vacancy is an exothermic process, also in the less favorable case in which the H atom is obtained by dissociation of H_2. The bonds with neighboring C atoms of the many isolated H atoms floating around in

diamond (for example in interstitial positions) is weaker than in H_2, and then the hydrogenation of VN_x becomes even more favorable.

As regards the second question, we focused here our attention on the C–H modes that appear at wavenumbers higher than 1340 cm^{-1}, and then far away from the Diamond+V+N manifold, characterized by a superposition of vibrational bands that form essentially a continuum. The 17 bending and the 10 stretching modes characterizing the systems here investigated span about 300 and 1000 cm^{-1}, respectively and should in principle be detectable individually, so as to allow to identify unambiguously all these defects.

However most of them do have a quite low intensity, so that they are hardly visible in the very rich IR experimental spectrum, to which many other kinds of defects are probably contributing. The only ones easily detectable in experiments are the peaks at 1405 (bending modes) and 3107 cm^{-1} (stretching mode), that have the largest computed intensities among bending and stretching (205 and 621 $km{\cdot}mol^{-1}$), and are now attributed unambiguously to the VN_3H defect.[5,9] The second most intense stretching peak (VN_2H_2) has intensity of 346 $km{\cdot}mol^{-1}$ (just a bit more than 50% of the one of VN_3H). The third one has intensity smaller than 200 $km{\cdot}mol^{-1}$; the remaining 7 peaks span from 20% of VN_3H, to nearly null intensity. Also in the bending region VN_3H has the most intense peak. The intensities of the VN_2H_2 and VNH_2 bending modes are not much lower than the one of VN_3H, and should in principle be visible. Looking at the forest of peaks appearing in the experimental spectra in the 1340 1600 cm^{-1} region (see for example the panels in figure 3 of ref 4), we decided that there are not enough elements for a one to one attribution of these peaks. It should be noticed that other defects can have intensity larger than the largest one of this set, and then generate large bands that can hidden the small peaks of the present systems.

We can conclude as follows:

1. Many of the defects here investigated (actually, all of them) can exist in defective diamond, but the evidence of their existence cannot be obtained for most of them from IR spectra.

2. The one to one correspondence between experimental and simulated spectra is difficult and prone to many errors for limitations on both sides (experiment and simulation). Fresher experiments might help in the comparison.

3. Simulation allows however to investigate *individually* and at well defined concentration each defect, and then should be used as a reference for a qualitative and semi-quantitative location of peak position and intensities for the various defects, also in the analysis and interpretation of experimental spectra.

ACKNOWLEDGEMENTS

SS and RD acknowledge the Cineca award (HP10CLF46D) under the Iscra initiative, for the availability of high performance computing resources and support. FSG acknowledge the Cineca awards (HP10BZSAHZ and HP10CTG8YY) under the Iscra initiative, for the availability of high performance computing resources and support.

[1] G. S. Woods and A. T. Collins. Infrared Absorption Spectra of Hydrogen Complexes in Type I Diamonds. *J. Phys. Chem. Solids*, 44(5):471–475, 1983.

[2] T. Hainschwang, F. Notari, E. Fritsch, and L. Massi. Natural, Untreated Diamonds Showing the A, B and C Infrared Absorptions ("ABC Diamonds"), and the H_2 Absorption. *Diam. Relat. Mater.*, 15(10):1555–1564, 2006.

[3] J. P. Goss, R. Jones, M. I. Heggie, C. P. Ewels, P. R. Briddon, and S. Öberg. Theory of Hydrogen in Diamond. *Phys. Rev. B*, 65(11):115207, 2002.

[4] E. Fritsch, T. Hainschwang, L. Massi, and B. Rondeau. Hydrogen-Related Optical Centers in Natural Diamond: an Update. *New Diamond Frontier Carbon Technol.*, 17(2):63–89, 2007.

[5] J. P. Goss, P. R. Briddon, V. Hill, R. Jones, and M. J. Rayson. Identification of the Structure of the 3107 cm^{-1} H-related Defect in Diamond. *J. Phys. Condens. Matter*, 26:145801, 2014.

[6] J. J. Charette. Essai de Classification des Bandes d'Absorption Infrarouge du Diamant. *Physica*, 27(11):1061–1073, 1961.

[7] C. E. Melton, A. A. Giardini, and C. A. Salotti. Observation of Nitrogen, Water, Carbon-Dioxide, Methane and Argon as Impurities in Natural Diamonds, 1972.

[8] R. M. Chrenko, R. S. McDonald, and K. A. Darrow. Infrared spectra of diamond coat. *Nature*, 213:474–476, 1967.

[9] F. Gentile, S. Salustro, M. Causá, A. Erba, P. Carbonniére, and R. Dovesi. The VN_3H Defect in Diamond. A Quantum Mechanical Investigation of the Structural, Electronic and Vibrational Properties. *Phys. Chem. Chem. Phys.*, 1(4):1–2, 2017.

[10] C. V. Peaker, J. P. Goss, P. R. Briddon, A. B. Horsfall, and M. J. Rayson. Di-Nitrogen–Vacancy–Hydrogen Defects in Diamond: a Computational Study. *Phys. Status Solidi A*, 212(11):2616–2620, 2015.

[11] J. P. Perdew and A. Zunger. Self-Interaction Correction to Density-Functional Approximations for Many-Electron Systems. *Phys. Rev. B*, 23(10):5048, 1981.

[12] J. Baima, A. Zelferino, P. Olivero, A. Erba, and R. Dovesi. Raman Spectroscopic Features of the Neutral Vacancy in Diamond from *Ab Initio* Quantum-mechanical Calculations. *Phys. Chem. Chem. Phys.*, 18(3):1961–1968, 2016.

[13] A. Zelferino, S. Salustro, J. Baima, V. Lacivita, R. Orlando, and R. Dovesi. The Electronic States of the Neutral Vacancy in Diamond: a Quantum Mechanical Approach. *Theor. Chem. Acc.*, 135(3):1–11, 2016.

[14] S. Salustro, A. Erba, C. M. Zicovich-Wilson, Y. Nöel, L. Maschio, and R. Dovesi. Infrared and Raman Spectroscopic Features of the Self-Interstitial Defect in Diamond from Exact-Exchange Hybrid DFT Calculations. *Phys. Chem. Chem. Phys.*, 120:21288–21295, 2016.

[15] S. Salustro, Y. Nöel, C. M. Zicovich-Wilson, P. Olivero, and R. Dovesi. The V+I Defects in Diamond: an *Ab Initio* Investigation of the Electronic Structure, of the Raman and IR Spectra, and of their Possible Recombination . *J. Chem. Phys.*, 145(18):184701, 2016.

[16] S. Salustro, G. Sansone, C. M. Zicovich-Wilson, Y. Noël, L. Maschio, and R. Dovesi. The A-center Defect in Diamond. A Quantum Mechanical Characterization Through the Infrared Spectrum. *Phys. Chem. Chem. Phys.*, 19:14478–14485, 2017.

[17] S. Salustro, A. M. Ferrari, F. S. Gentile, J. K. Desmarais, M. Rérat, and R. Dovesi. Characterization of the B-center Defect in Diamond Through the Vibrational Spectrum. A Quantum Mechanical Approach. *J. Phys. Chem. A*, 2017.

[18] S: Salustro, A. M. Ferrari, R. Orlando, and R. Dovesi. Comparison Between Cluster and Supercell Approaches: the case of Defects in Diamond. *Theor. Chem. Acc.*, 4(136):1–13, 2017.

[19] S. Salustro, F. S. Gentile, P. D'Arco, B. Civalleri, M. Rérat, and R. Dovesi. Hydrogen Atoms in the Diamond Vacancy Defect. A Quantum Mechanical Vibrational Analysis. *Carbon*, 2017.

[20] G. Sansone, S. Salustro, Y. Noël, L. Maschio, W. C. Mackrodt, and R. Dovesi. Looking for sp^2 Carbon Atoms in Diamond: a Quantum Mechanical Study of Interacting Vacancies. *Theor. Chem. Acc.*, 137(2):29, 2018.

[21] A. D. Becke. Density-Functional Thermochemistry. III. The Role of Exact Exchange. *J. Chem. Phys.*, 98(7):5648–5652, 1993.

[22] C. Lee, W. Yang, and R. Parr. Development of the Colle-Salvetti Correlation-Energy Formula Into a Functional of the Electron Density. *Phys. Rev. B*, 37(2):785–789, 1988.

[23] R. Dovesi, A. Erba, R. Orlando, C. M. Zicovich-Wilson, B. Civalleri, L. Maschio, M. Rérat, S. Casassa, J. Baima, S. Salustro, and B. Kirtman. Quantum-Mechanical Condensed Matter Simulations with CRYSTAL. *Wires*, 2018. *Accepted.*

[24] W. J. Hehre, R. Ditchfield, and J. A. Pople. SelfConsistent Molecular Orbital Methods. XII. Further Extensions of GaussianType Basis Sets for Use in Molecular Orbital Studies of Organic Molecules. *J. Chem. Phys.*, 56(5):2257–2261, 1972.

[25] R. Dovesi, V. R. Saunders, C. Roetti, R. Orlando, C. M. Zicovich-Wilson, F. Pascale, B. Civalleri, K. Doll, N. M. Harrison, I. J. Bush, Ph. D'Arco, and M. Llunell. *CRYSTAL 2014 User's Manual.* . University of Torino, Torino, 2013.

[26] H. J. Monkhorst and J. D. Pack. Special Points for Brillouin-Zone Integrations. *Phys. Rev. B*, 13(12):5188, 1976.

[27] F. Pascale, C. M. Zicovich-Wilson, F. Lòpez Gejo, B. Civalleri, R. Orlando, and R. Dovesi. The Calculation of the Vibrational Frequencies of the Crystalline Compounds and its Implementation in the CRYSTAL Code. *J. Comput. Chem.*, 25(6):888–897, 2004.

[28] C. M. Zicovich-Wilson, F. Pascale, C. Roetti, V. R. Saunders, R. Orlando, and R. Dovesi. Calculation of the Vibration Frequencies of α-Quartz: The Effect of Hamiltonian and Basis Set. *J. Comput. Chem.*, 25(15):1873–1881, 2004.

[29] A. Erba, M. Ferrabone, R. Orlando, and R. Dovesi. Accurate Dynamical Structure Factors from *Ab Initio* Lattice Dynamics: The case of Crystalline Silicon. *J. Comput. Chem.*, 34:346–354, 2013.

[30] C. Carteret, M. De La Pierre, M. Dossot, F. Pascale, A. Erba, and R. Dovesi. The Vibrational Spectrum of $CaCO_3$ Aragonite: a Combined Experimental and Quantum-Mechanical Investigation. *J. Chem. Phys.*, 138(1):014201, 2013.

[31] J. Baima, M. Ferrabone, R. Orlando, A. Erba, and R. Dovesi. Thermodynamics and Phonon Dispersion of Pyrope and Grossular Silicate Garnets from *Ab Initio* Simulations. *Phys. Chem. Minerals*, 43:137–149, 2016.

[32] F. Pascale, C. M. Zicovich-Wilson, R. Orlando, C. Roetti, P. Ugliengo, and R. Dovesi. Vibration Frequencies of $Mg_3Al_2Si_3O_{12}$ Pyrope. An *Ab Initio* Study with the CRYSTAL Code. *J. Phys. Chem. B*, 109(13):6146–6152, 2005.

[33] F. Pascale, P. Ugliengo, B. Civalleri, R. Orlando, Ph. DArco, and R. Dovesi. Hydrogarnet Defect in Chabazite and Sodalite Zeolites: A Periodic Hartree–Fock and B3-LYP Study. *J. Chem. Phys.*, 117(11):5337–5346, 2002.

[34] R. Orlando, F. J. Torres, F. Pascale, P. Ugliengo, C. M. Zicovich-Wilson, and R. Dovesi. Vibrational Spectrum of Katoite $Ca_3Al_2[(OH)_4]_3$: a Periodic *Ab Initio* Study. *J. Phys. Chem. B*, 110:692–701, 2006.

[35] F. Pascale, S. Tosoni, C. M. Zicovich-Wilson, P. Ugliengo, R. Orlando, and R. Dovesi. Vibrational Spectrum of Brucite $Mg(OH)_2$: a Periodic *Ab Initio* Quantum Mechanical Calculation Including OH Anharmonicity. *Chem. Phys. Lett.*, 396:308–315, 2004.

[36] S. Tosoni, F. Pascale, P. Ugliengo, R. Orlando, V. R. Saunders, and R. Dovesi. Quantum Mechanical Calculation of the OH Vibrational Frequency in Crystalline Solids. *Molecular Physics*, 103(18):2549–2558, 2005.

[37] R. Demichelis, Y. Noël, B. Civalleri, C. Roetti, M. Ferrero, and R. Dovesi. The vibrational spectrum of α-alooh diaspore: an *Ab Initio* study with the CRYSTAL code. *J. Phys. Chem. B*, 111(31):9337–9346, 2007.

[38] M. Mérawa, P. Labeguerie, P. Ugliengo, K. Doll, and R. Dovesi. The Structural, Electronic and Vibrational Properties of LiOH and NaOH: an *Ab Initio* Study. *Chem. Phys. Lett.*, 387(4):453–459, 2004.

[39] P. Ugliengo, F.Pascale, M. Merawa, P. Labéguerie, S. Tosoni, and R. Dovesi. Infrared Spectra of Hydrogen-Bonded Ionic Crystals: *Ab Initio* Study of $Mg(OH)_2$ and β-$Be(OH)_2$. *J. Phys. Chem. B*, 108(36):13632–13637, 2004.

[40] G. M. Barrow. *Introduction to Molecular Spectroscopy.* McGraw-Hill, New York, 1962.

[41] B. A. Hess, L. J. Schaad, P. Carsky, and R. Zahradnik. *Ab Initio* Calculations of Vibrational Spectra and Their Use in the Identification of Unusual Molecules. *Chem. Rev.*, 86:709–730, 1986.

[42] L. Maschio, B. Kirtman, R. Orlando, and M. Rérat. *Ab Initio* Analytical Infrared Intensities for Periodic Systems Through a Coupled Perturbed Hartree-Fock/Kohn-Sham Method. *J. Chem. Phys.*, 137(20):204113, 2012.

[43] L. Maschio, B. Kirtman, M. Rérat, R. Orlando, and R. Dovesi. Comment on "*Ab Initio* Analytical Infrared Intensities for Periodic Systems Through a Coupled Perturbed Hartree-Fock/Kohn-Sham Method" [J. Chem. Phys. 137, 204113 (2012)]. *J. Chem. Phys.*, 139:167101, 2013.

[44] D.A. McQuarrie and J.D. Simon. *Physical Chemistry. A*

Molecular Approach. University Science Books, Sausalito, CA, 1977.

[45] J. L. Duncan, D. C. McKean, I. Tortoand A. Brown, and A. M. Ferguson. Infrared Studies of CH and CD Stretching Anharmonicity. *Journal of the Chemical Society, Faraday Transactions 2: Molecular and Chemical Physics*, 84(9):1423–1442, 1988.

[46] M. L. Myrick, A. E. Greer, A. A. Nieuwland, R. J. Priore, J. Scaffidi, D. Andreatta, and P. Colavita. Birge–Sponer Estimation of the C–H Bond Dissociation Energy in Chloroform Using Infrared, Near-Infrared, and Visible Absorption Spectroscopy. An Experiment in Physical Chemistry. *J. Chem. Educ*, 85(9):1276, 2008.

[47] P. Ugliengo. ANHARM. A Program to Solve Monodimensional Nuclear Schroedinger Equation. *Unpublished*, 1989.